Joule heating patterns as a function of polar cap index

Francis K. Chun, Delores J. Knipp, Matthew G. McHarg, and James R. Lacey
Department of Physics, U.S. Air Force Academy, Colorado, USA

Gang Lu and Barbara A. Emery
High Altitude Observatory, National Center for Atmospheric Research, Boulder, Colorado, USA

Received 31 July 2001; revised 17 December 2001; accepted 19 December 2001; published 20 July 2002.

[1] Previous work by *Chun et al.* [1999] has shown that the polar cap (PC) index can be used as a proxy indicator of the integrated Joule heating rate in the Northern Hemisphere. However, knowledge of the spatial distribution of Joule heating is also important. The PC index is a single magnetometer station-derived index which measures the level of geomagnetic activity in the polar cap. A negative PC index corresponds to a condition related to lobe-merging convection conditions in the polar cap, near-zero PC indicates a quiet polar cap, and a positive PC indicates geomagnetically active periods. In this study we developed average patterns of Joule heating as a function of PC using 56 days (~12,800 individual patterns) of Assimilative Mapping of Ionospheric Electrodynamics data from various case studies. With PC ranging from −3 to 8, we divide the Joule heating patterns into PC bins of 1.0, finding that there is a clear spatial evolution of Joule heating from negative PC to positive PC. When PC is negative, Joule heating on average is constrained to the high-latitude dayside. As PC goes to zero, Joule heating disappears. When PC increases in the positive direction, Joule heating intensifies throughout the auroral oval, with primary heating occurring along the dawn/dusk flanks. Further analysis reveals that it is primarily changes in the electric potential and not the Pedersen conductance that accounts for Joule heating shifting from the auroral zone to the high-latitude dayside when PC goes negative. We also find that the cross polar cap potential is linearly proportional to the PC index, consistent with previous studies. Finally, we compare the hemispheric energy budget between Joule heating and electron particle energy. We find that globally, Joule heating is roughly 4 times that of particle energy during geomagnetically active times (positive PC). During quiet times (zero PC), Joule heating and particle energy are equal contributors. When lobe-merging conditions occur (negative PC), Joule heating again dominates over particle energy except during the winter season, when polar cap conductivity is driven more by particle precipitation. *INDEX TERMS:* 2431 Ionosphere: Ionosphere/magnetosphere interactions (2736); 2736 Magnetospheric Physics: Magnetosphere/ionosphere interactions; 2437 Ionosphere: Ionospheric dynamics; *KEYWORDS:* Joule heating, particle heating, ionosphere, polar cap index, Assimilative Mapping of Ionospheric Electrodynamics (AMIE)

1. Introduction

[2] Joule heating is resistive heating due to current flow along an electric field. The classic example of Joule heating is the heat one feels from an incandescent light bulb. Joule heating of Earth's upper atmosphere causes expansion of the atmosphere and leads to a variety of dynamic and chemical changes in the atmosphere and increased drag on low Earth-orbiting satellites. Previous studies have focused on developing simple relationships between the total heating in the Northern Hemisphere to various ionosphere properties or geomagnetic indices [e.g., *Chun et al.*, 1999; *Ahn et al.*, 1983; *Baumjohann and Kamide*, 1984]. Although important to know the total Joule heating in the upper atmosphere, it is critical to know where the heating is occurring. Joule heating patterns provide such insight.

[3] Creating hemisphere Joule heating patterns can prove to be a daunting task because the patterns require detailed spatial knowledge of heating parameters. Only *Foster et al.* [1983] have published averaged Joule heating patterns as a function of geomagnetic activity. These patterns were based on simultaneous observations of the electric field and Pedersen conductivity calculated from individual measurements of the ion drift velocity and particle precipitation observed over the lifetime of the Atmospheric Explorer (AE-C) satellite from 1974 to 1978. The patterns were of a spatial resolution of 5° latitude by 2-hour local time and were categorized by season (spring, summer, autumn, and winter) and the *Kp* index (*Kp* = 0−3 and 3−6).

0148-0227/02/2001JA000246$09.00

[4] We now have a unique opportunity to develop higher spatial and geomagnetic activity resolution patterns of Joule heating and associated ionosphere properties using data from the Assimilative Mapping of Ionospheric Electrodynamics (AMIE) technique. The AMIE technique is a weighted least-squares fit of ionospheric electrodynamic parameters to a variety of ground- and space-based data and statistical models [*Richmond and Kamide*, 1988]. The procedure is typically run at a 5–10 min cadence, thus producing time-varying maps of high-latitude features. The a priori information contained in the statistical models is used to constrain the electrodynamic parameters over regions where data are absent or sparse.

[5] The procedure first modifies statistical models of ionospheric height-integrated conductance and auroral precipitation with all available observations related to these parameters. The newly derived conductance distribution is applied to the inversion of ground magnetic perturbations to help produce the electric potential or convection distribution. When available, more direct information about the electric field, such as ion drift observations from polar orbiting satellites and radars, are assimilated with magnetic perturbations to create a global view of the high-latitude electrodynamics. The weighting factors for the observations are given by the inverse covariance matrix of the errors, including observational errors, errors associated with AMIE's inherent spatial smoothing, and errors associated with inaccuracies in the simplifying assumptions that are used within the procedure. The errors are presumed to be uncorrelated.

[6] In the past, AMIE has been used extensively for geomagnetic storm case studies, some which have focused on electric field and conductance distributions. These studies have provided a wealth of data that can be used to produce patterns of many ionosphere properties. For this study we extract two additional AMIE output fields that are directly relevant to estimating the energy dissipation in the ionosphere, precipitating electron energy flux and Joule heating. AMIE calculates Joule heating as $\Sigma_p E^2$, where Σ_p is the height-integrated Pedersen conductivity in the ionosphere and E is the electric field.

[7] In this paper we present results of our study, which not only shows expected hemisphere patterns during most geomagnetic conditions but also averaged heating patterns during periods of lobe merging. We use the polar cap (PC) index as a measure of geomagnetic activity as opposed to more established indices such as *AE*. *Vennerstrøm et al.* [1991] discussed reasons why one would sometimes want to use PC over *AE*. In this study we use PC because this work is an extension of our previous work and because PC is available in near real time. Thus we extend our previous study [*Chun et al.*, 1999], which showed that the polar cap index can be used as a proxy measurement of the hemispheric, integrated Joule heating rate into the domain of spatial variations. We first discuss our data and then present local time and latitude maps of Joule heating as a function of the polar cap index. Finally, we compare our results to previous studies and discuss our limitations.

2. Data

[8] The polar cap index is derived from a single magnetometer located in the polar cap region [*Troshichev et al.*, 1988] and is a measure of geomagnetic activity level in the polar cap. The north PC index is derived from a magnetometer station at Thule, while the south PC index is derived from the Vostok station. PC is well correlated to Joule heating [*Chun et al.*, 1999] and to the *AE* index [*Vennerstrøm et al.*, 1991] and is reported at a 15-min time resolution. In our study we use the PC index values calculated from the Qaanaq (Thule) ground magnetometer operated by the Danish Meteorological Institute (DMI). DMI processes the PC index using 12 (months) by 24 (hours) coefficients and a winter-time quiet level curve removal method. Some evidence exists that a 5-min coefficient set and a different quiet level curve removal would produce larger PC values (O. Troshichev, personal communication, 2001). We believe that our binning of PC is minimally affected by the choice of PC processing methods. Figure 1 shows the cumulative sum distribution of PC in our database. Most of the time the PC index indicates low to moderate activity (PC = 0–5) and only rarely (<10% of patterns) records extreme storm (>5) or lobe-merging convection (<0) activity.

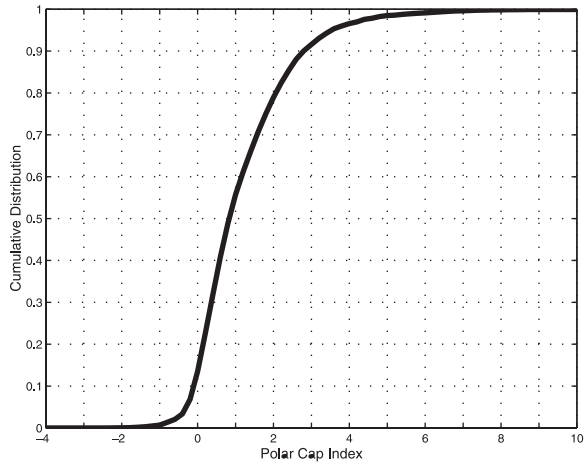

Figure 1. Cumulative distribution of the polar cap (PC) index in our database.

[9] Table 1 summarizes the AMIE case studies that we have used in this study. These studies include magnetometer data from at least 60 stations worldwide with between 3 and 5 stations in the polar cap. Many of these studies also use data from various satellites such as TIROS, DMSP, Akebono (EXOS D), and UARS. Typical satellite data included in AMIE studies are electron precipitation data and ion drift measurements. Finally, most of these studies use data from coherent and incoherent radar (e.g., ion drift velocities), and a few used data from polar cap digisondes. Details of the case studies and their data input are given by the associated references.

[10] The campaigns tended to focus on geomagnetically active periods. Can they be considered representative of the broader realm of solar-terrestrial interactions? In Table 1 we have used data from a solar flow characterization study [*Richardson et al.*, 2000; I. Richardson, personal communication, 2001] to show the number of hours in each campaign interval associated with three solar flow types:

Table 1. Events Used in This Study

	Solar Wind Flow Type, Hours			
	Ejecta	High-Speed Flow	Slow Flow	Source[a]
Date				
12–16 January 1988	72(MC)[b]	48		4
20–21 March 1990	24		24	2, 12, 13
2–3 August 1991		48		15
8–9 November 1991	48			1
27–29 January 1992	24		48	8
28–29 March 1992			48	9, 10
20–21 July 1992		36	12	11
16–17 February 1993	24	24		16
27 May 1993		24		6
2–11 November 1993	24	144	72	5
18–23 October 1995	36(MC)	72	36	3
26–29 May 1996	36(MC)	48	12	3
9–13 January 1997	30(MC)	72	18	7
9–13 April 1997	84(MC)		36	15
14–18 May 1997	72(MC)			14
Total hours, 1344	474	516	354	
Percentage	35.3	38.4	26.3	
Solar cycle average, %	30	45	25	

[a]Sources are as follows: 1, *Cooper et al.* [1995]; 2, *Crowley et al.* [2000]; 3, *Farrugia et al.* [1998]; 4, *Knipp et al.* [1993]; 5, *Knipp et al.* [1998]; 6, *Kobea et al.* [2000]; 7, *Lu et al.* [1998]; 8, *Lu et al.* [1994]; 9, *Lu et al.* [1995]; 10, *Lu et al.* [1996]; 11, *Pinnock et al.* [1999]; 12, *Taylor et al.* [1996]; 13, *Taylor et al.* [1997]; 14, G. Le et al., Strong IMF by related plasma convection in the ionospheric cusp field-aligned currents under northward IMF conditions, submitted to *Journal of Geophysical Research*, 2002; 15, G. Lu, unpublished data, 2001; and 16, B. Emery, unpublished data, 1998.

[b]MC stands for magnetic cloud.

ejecta, high-speed stream, and slow flow. In our database, 35.3% of the campaign hours were dominated by ejecta, 38.4% by high-speed flow, and 26.3% by slow flow. Solar cycle averages for these flow types are 30% ejecta, 45% high-speed flow, and 25% slow flow. While the AMIE intervals proportionately represent slow flow, ejecta are slightly over-represented, and high-speed streams are somewhat underrepresented. Despite this the distribution of PC index associated with our database is very similar to the overall PC distribution for 1975–1997 (see discussion below). We believe that this arises because many of our ejecta events are magnetic clouds with significant intervals of a northward interplanetary magnetic field that produces geomagnetic quiet conditions even though Earth is immersed in ejecta flow. Although the case studies were usually solar and geomagnetic events, we feel that they provide a good representative sampling of ionospheric conditions.

[11] *Chun et al.* [1999, Figure 1] showed the cumulative distribution of the PC index for three situations: an active year (1982) based on the sunspot number, a quiet year (1997), and the average of all the PC data available at the time (1975–1997). What that figure showed was that, on average, PC > 5 occurred ~2–3% of the time, and PC < 0 occurred ~7–8% of the time. It also showed a median (0.5 or 50%) PC value of just under 1. The distribution of the PC index in our database is very similar as seen in Figure 1 and in Table 2. Table 2 is a breakout of the percentage of AMIE patterns in our database per PC bin. It is clear from Table 2 that most of the AMIE patterns correspond to low to moderate PC values ($0 \leq PC < 5$). Looking at the "percent of total" numbers for the negative and large positive PC (PC < 0 and PC > 5, respectively) across all three seasons, one sees that 9.4% of the patterns fall into those extreme PC ranges. Finally, the median PC value in our database is also just under 1.

[12] Since the case studies were at various time and spatial resolutions, we merged the data for our study into 2° magnetic colatitude by 1-hour magnetic local time (MLT) bins. We did, however, maintain the time resolution of the AMIE data and interpolated the Northern Hemisphere PC data from Thule from 15 min to the appropriate AMIE time resolution (either 5 or 10 min). Our database consists of 56 days and ~12,800 individual patterns. Using bin sizes of 1 in PC (from −3 to 8), we took the average of the individual patterns for each bin. We also divided our patterns into a summer, winter, and equinox season defined by a window of ~90 days centered on the appropriate solstice and equinox.

3. Joule Heating Patterns

[13] Figures 2, 3, and 4 are the Joule heating patterns for summer, equinox, and winter, respectively. These patterns represent the average of all patterns which fall into each PC bin. The patterns are arranged from the most negative PC bin for the season (top left) to the most positive PC bin (bottom right) in a left-to-right fashion. Magnetic noon local time is at the top, and midnight local time is at the bottom for each individual pattern. The latitude scale is from 40° to 90°. The number of individual AMIE patterns included in the averaged pattern is indicated by the number in parentheses, and the total integrated hemisphere Joule heating is calculated and presented with each average pattern (for example, for the pattern corresponding to PC index between 0 and 1 in the summer, there are 1716 individual patterns that went into the averaged pattern, and its integrated Joule heating rate is 24 GW). The colorscale of the Joule heating contours range from 0.001 to 0.08 W/m^2 with a contour interval of 0.002 W/m^2.

[14] Figure 2 shows a progression of average Joule heating patterns (read left to right, top to bottom) in the Northern Hemisphere during the summer season for negative PC (lobe-merging convection conditions), zero to low positive PC (quiet geomagnetic conditions), and large positive PC (active geomagnetic conditions). PC ranges from −3 to 6. There is a clear evolution of the Joule heating spatial distribution from the high-latitude dayside (dayside defined as sunward of the dawn-dusk meridian) to an auroral oval shape as the polar cap activity changes from a lobe-merging

Table 2. Data Coverage

	Summer		Equinox		Winter	
	Season, %	Total, %	Season, %	Total, %	Season, %	Total, %
PC Index						
$-3 \leq PC < -2$	0.08	0.02				
$-2 \leq PC < -1$	0.75	0.22	0.48	0.20	0.13	0.04
$-1 \leq PC < 0$	11.59	3.39	8.21	3.31	4.68	1.42
$0 \leq PC < 1$	45.83	13.41	35.91	14.50	46.25	14.05
$1 \leq PC < 2$	25.08	7.34	24.57	9.92	27.52	8.36
$2 \leq PC < 3$	11.83	3.46	17.91	7.23	12.33	3.74
$3 \leq PC < 4$	3.13	0.91	7.63	3.08	5.46	1.66
$4 \leq PC < 5$	1.28	0.38	3.21	1.30	1.67	0.51
$5 \leq PC < 6$	0.43	0.13	0.91	0.37	0.88	0.27
$6 \leq PC < 7$			0.72	0.29	0.82	0.25
$7 \leq PC < 8$			0.45	0.18	0.26	0.08
Subtotal, %	100	29.26	100	40.38	100	30.38

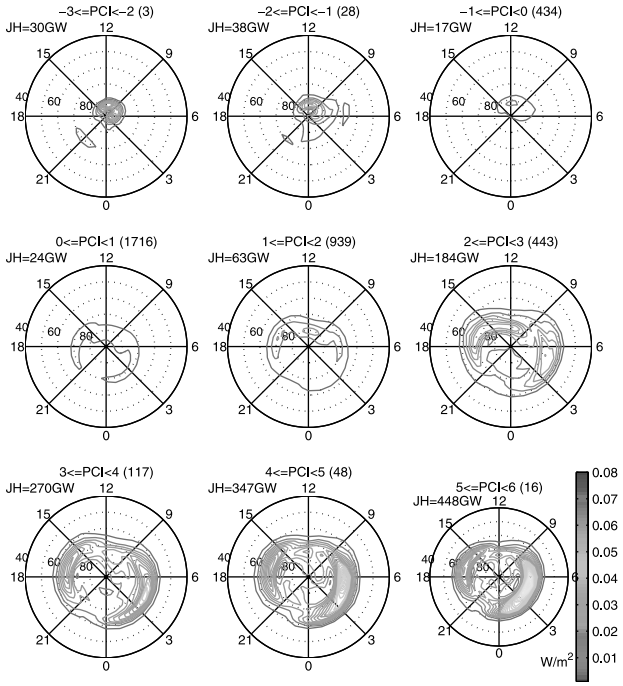

Figure 2. Average Joule heating patterns as a function of polar cap index (summer). See color version of this figure at back of this issue.

convection condition to an active geomagnetic level. In addition, the total integrated Joule heating rate also increases in both directions away from the quiet condition (PC = 0). During negative PC periods the total integrated heating rate increases from ~17 to 38 GW and is constrained to a very localized region in the high-latitude dayside. As PC increases, the total heating rate increases to ~450 GW and becomes more intense along the dawn and dusk flanks, with the predominate heating occuring on the dawn side.

[15] Figure 3 shows the average Joule heating patterns for equinox (which includes both spring and autumn). For the equinox patterns, PC ranges from −2 to 8 (again, read from left to right, top to bottom). A comparison with Figure 2 shows no substantial difference between summer and equinox patterns. As with the summer patterns, the equinox Joule heating patterns exhibit localized heating in the high-latitude dayside during negative PC intervals, minimal Joule heating for near-zero PC conditions, and increased intensity and spatial extent along the auroral oval for larger positive PC values. The total integrated heating varies from 16 to 317 GW.

[16] Figure 4 is the average Joule heating patterns for winter with PC ranging from −2 to 8. Compared with summer and equinox, there are fewer cases when PC is strongly negative, but even during slightly negative PC values ($-1 \leq PC < 0$), Joule heating, on average, occurs at high latitudes on the dayside. However, for the most negative PC bin ($-2 \leq PC < -1$), there is, on average, no strong region of heating except for a narrow latitudinal region along the dusk meridian. As PC increases, however, Joule heating is again constrained to the auroral oval with intense heating occuring more along the dawn flank than the dusk flank. The total integrated Joule heating ranges from 4 to over 450 GW.

[17] In the presentation of these average patterns a question arises as to whether the average results are statistically significant. Another question is whether the PC index orders the Joule heating data well. We attempt to assess the statistical significance of the Joule heating data by analyzing how the average Joule heating rate (mW/m^2) varies as a function of PC for four different latitude local time sectors. The four sectors were located at midnight (78°−84° magnetic latitude (MLAT), 22−02 MLT), noon (78°−84° MLAT, 10−14 MLT), dawn (60°−66° MLAT, 04−08 MLT), and dusk (60°−66° MLAT, 16−20 MLT). These four latitude local time sectors were chosen to represent the high-latitude polar regions along the noon-midnight meridian and the auroral region along the flanks of the ionosphere, respectively.

[18] Figure 5 shows the average Joule heating rate as a function of PC for these four sectors. The midnight sector is the top panel, noon is the second panel, dawn is the third panel, and dusk is the bottom panel. The data are further separated into summer (left column; Figure 5a), equinox (middle column; Figure 5b), and winter (right column; Figure 5c) seasons. Note the different y axis scales for the midnight and noon plots (−5 to 20 mW/m^2) compared to the dawn and dusk plots (−10 to 40 mW/m^2). All of the plots have the same x axis scale ($-3 \leq PC < 9$). All four latitude local time sectors in each season show that the

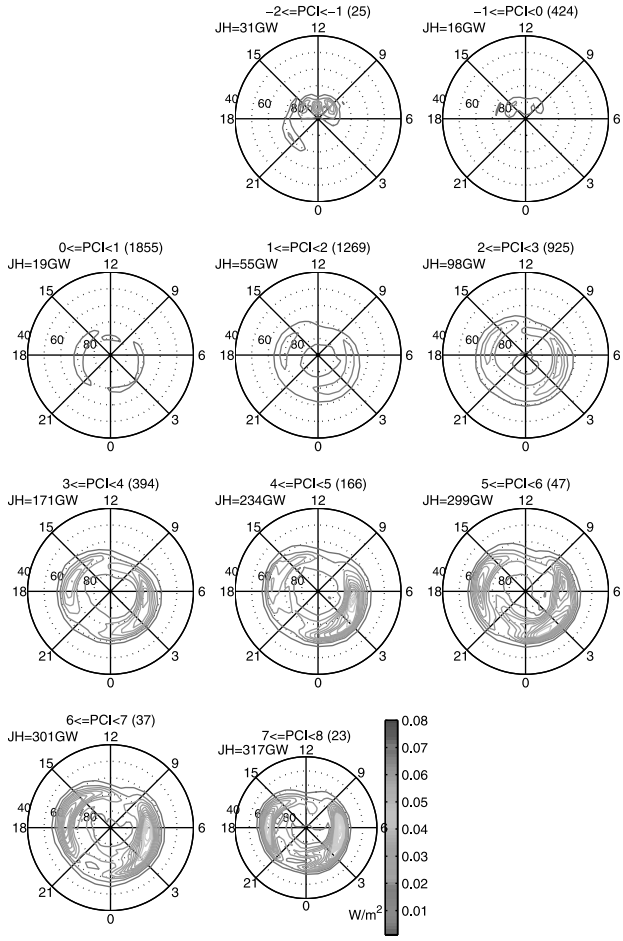

Figure 3. Average Joule heating patterns as a function of PC index (equinox). See color version of this figure at back of this issue.

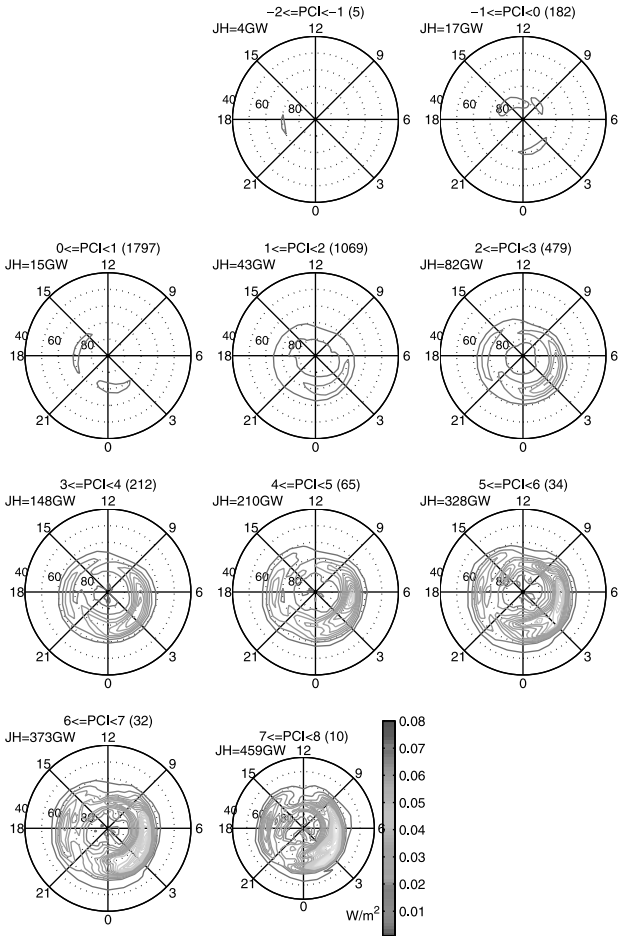

Figure 4. Average Joule heating patterns as a function of PC index (winter). See color version of this figure at back of this issue.

average Joule heating is minimal around a PC of zero since the activity is low. However, as activity increases in the positive PC direction, the average Joule heating also increases in all four latitude local time sectors and in all seasons. As one would expect, the dawn and dusk flanks exhibit the highest heating compared to the high-latitude midnight and noon sectors. However, the noon plots show that significant heating can occur at higher latitudes as PC becomes negative (indicative of northward IMF conditions). Also of note is the asymmetry in the dawn and dusk heating rates. The average dawn heating rate can at times be about twice that of the dusk heating rate. Thus Figure 5 suggests that our results are statistically significant in that each sector responds differently with PC, each latitude local time sector's relationship with PC varies across seasons, and that PC orders the Joule heating data well.

4. Discussion

4.1. Heating Associated With Lobe-Merging Convection

[19] Analysis of the averaged Joule heating patterns during lobe-merging convection periods (negative PC) shows that much of the heating is constrained to very high latitudes and to the dayside, as opposed to occurring along the auroral oval and flanks. This result indicates that the classic two-cell convection pattern evolves into a smaller spatial region with no discernable auroral oval as the conditions in the polar cap evolve into a lobe-merging convection situation.

[20] To investigate this further, we present representative averaged patterns of the electric potential and Pedersen conductance for three PC bins. Figure 6 shows a series of averaged Pedersen conductance (top row) and electric potential (middle row) patterns associated with the Joule heating patterns for the summer season and the three negative PC bins from −3 to 0 (i.e., the top row of Joule heating patterns from Figure 2). Note that the bottom row of Figure 6 also shows corresponding average patterns of electron particle fluxes, which will be discussed in section 4.2. The format of the plots are similar to the Joule heating pattern plots, except that for the electric potential plots the cross polar cap potential is reported. The three patterns in the $-3 \leq PC < -2$ plot are from the 26–29 May 1996 event; the 28 patterns in the $-2 \leq PC < -1$ plot are from the 2–3 August 1991 (5 patterns), 26–29 May 1996 (21 patterns), and 27 May 1993 (2 patterns) events; and the 434

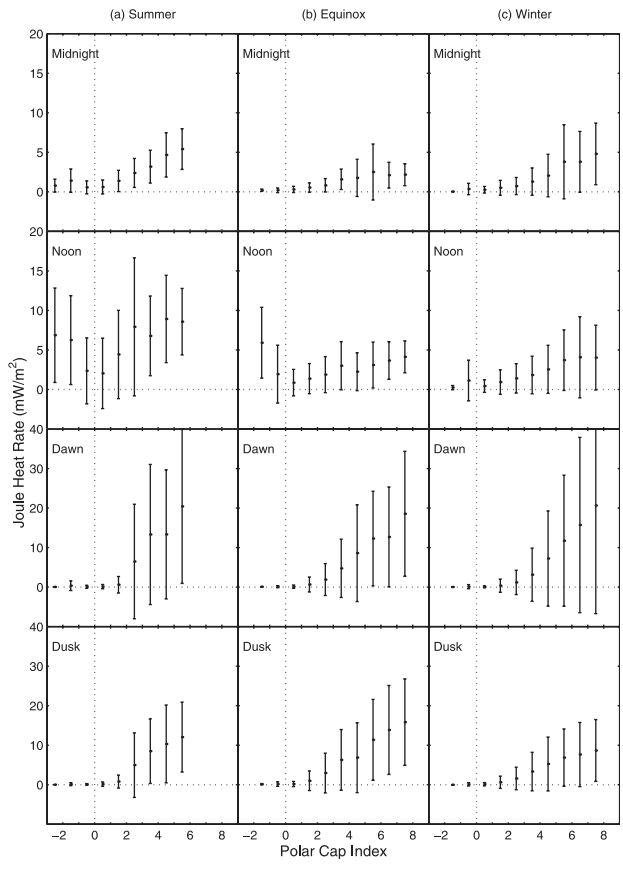

Figure 5. Average Joule heating rate (mW/m^2) for midnight, noon, dawn, and dusk segments as a function of PC. (a) Summer data is shown in the left column, (b) equinox is shown in the middle column, and (c) winter is shown in the right column. The standard deviation of the average are also plotted as the error bars, but the reader is cautioned that negative Joule heating is unphysical.

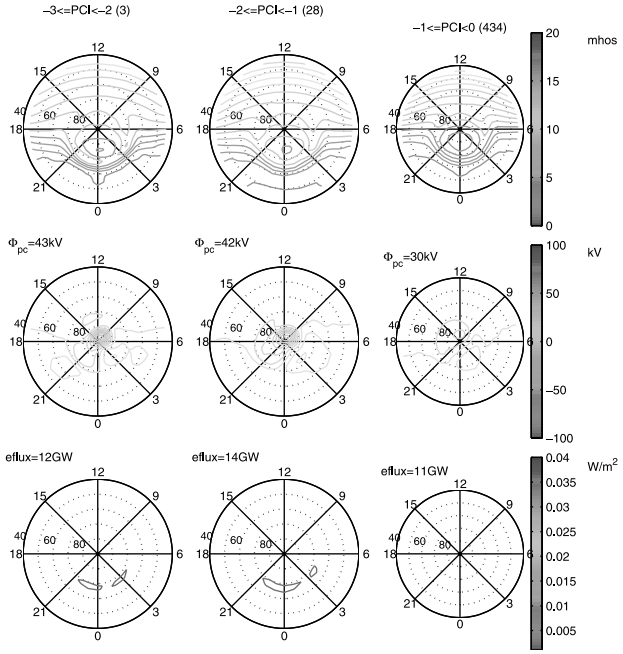

Figure 6. Average Pedersen conductance and electric potential patterns associated with the averaged Joule heating summer patterns (top row of plots in Figure 2) for negative PC ($-2.5 \leq PC < -0.5$). The average electron particle flux patterns corresponding to the same PC bins are plotted in the bottom row. See color version of this figure at back of this issue.

patterns in the $-1 \leq PC < 0$ plot are from the 2–3 August 1991 (10 patterns), 20–21 July 1992 (62 patterns), 27 May 1993 (50 patterns), 26–29 May 1996 (176 patterns), and 14–18 May 1997 (136 patterns) events.

[21] The averaged Pedersen conductance patterns (Figure 6, top row) do not show any dramatic evolution from a PC of −3 to a PC of 0 (especially in the high-latitude dayside). In addition, although there is significant distortion of the solar-induced conductivity, there is no noticeable enhancement of conductivity at high latitudes on the dayside. The primary factor constraining Joule heating to the high-latitude dayside appears to be the electric fields, as seen in the electric potential patterns. Granted, the averaged electric potential, and thus Joule heating patterns, for the first two PC bins are dominated by the 26–29 May 1996 event. Thus one would expect very little change in the average patterns. However, the third plot ($-1 \leq PC < 0$) is not as heavily dominated by the 26–29 May 1996 event, and we can observe that although the averaged electric potential pattern is different from the previous PC bins, the result is the same: The average Joule heating is still confined to the high-latitude region.

[22] Previous work by *Foster et al.* [1983] showed high-latitude dayside heating (note that their data were limited to latitudes <80°) usually comparable to or greater than that along the auroral oval. Their averaged patterns exhibited global heating occuring throughout all seasons and geomagnetic activity ($Kp = 0–3$ and 3–6), whereas our patterns show a clear evolution with the PC index from polar cap or high-latitude dayside heating to intense heating in the dusk/dawn flanks of the oval. This difference in our patterns is probably due to differences in our geomagnetic binning scheme and parameter since the *Kp* index is not as well suited as the PC index in distinguishing lobe-merging convection conditions. *Foster et al.* [1983] also showed heating rates between 0 and 8 mW/m^2 with total integrated heating rates upward to 160 GW, lower than our estimates by up to a factor of 4. We find that our integrated hemispheric Joule heating rate is more comparable to those found by *Ahn et al.* [1983] and *Baumjohann and Kamide* [1984].

4.2. Comparison Studies

[23] We make a simple comparison of integrated Joule heating rates for each season and averaged pattern to the quadratic fits from our earlier study [*Chun et al.*, 1999] in Figure 7. The average integrated heating rate and standard deviation (indicated by the error bars) of each PC bin are plotted as the data points, and a quadratic fit is plotted as the solid line. Since the fit relationships intercept the majority of the error bars, one could make the argument that the quadratic fits appear to adequately represent this study's results. This is expected though since the fits were based on a subset of the database used in this study. This study includes data from two severe storm events ($Kp > 8$) that were excluded from our earlier study due to less than ideal satellite data coverage.

[24] Using data from the low-energy charged particle detector and the electric field detector on the EXOS D (Akebono) satellite, *Troshichev et al.* [1996] correlated the cross polar cap potential to the PC index. Using 80 EXOS D crossings of the polar cap in March–April 1990, they found a correlation of 0.797 between the two parameters with a relationship of $\Phi(kV) = 19.35\ PC + 8.78$. We have average electric potential patterns (e.g., middle row of Figure 6) for each Joule heating pattern as a function of PC, so we can also correlate the average cross polar cap potential from the AMIE database to the PC index. Figure 8 shows our results for each season, summer (top panel), equinox (middle panel), and winter (bottom panel). We show two correlations, one for positive PC and one for negative PC. In addition, we show the *Troshichev et al.* [1996] correlation as a dashed line.

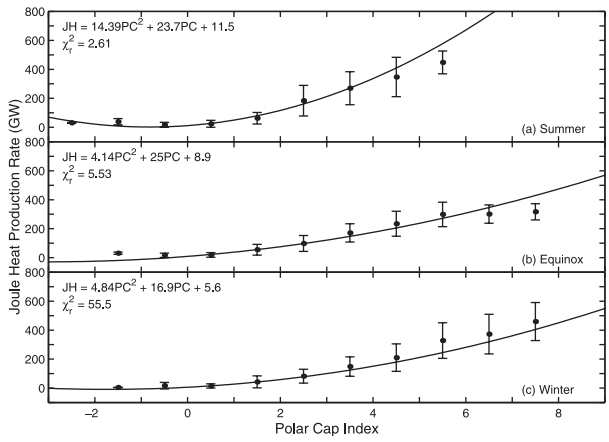

Figure 7. Comparison of integrated Joule heating from average patterns with quadratic fits (proxy Joule heating) [from *Chun et al.*, 1999].

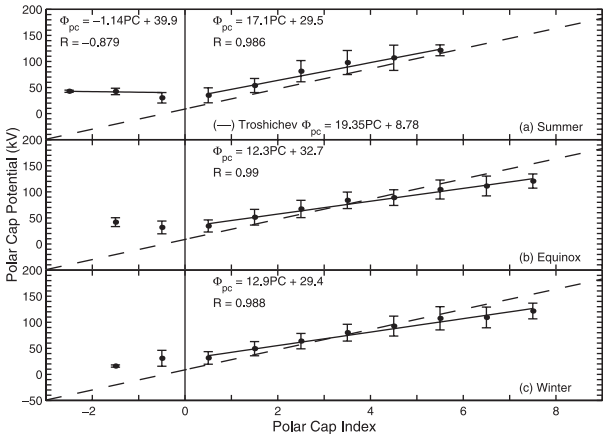

Figure 8. Relationship between cross polar cap potential and PC. The top panel shows summer, the middle shows equinox, and the bottom shows winter. The linear fit (dashed line) from *Troshichev et al.* [1996] is also shown for comparison.

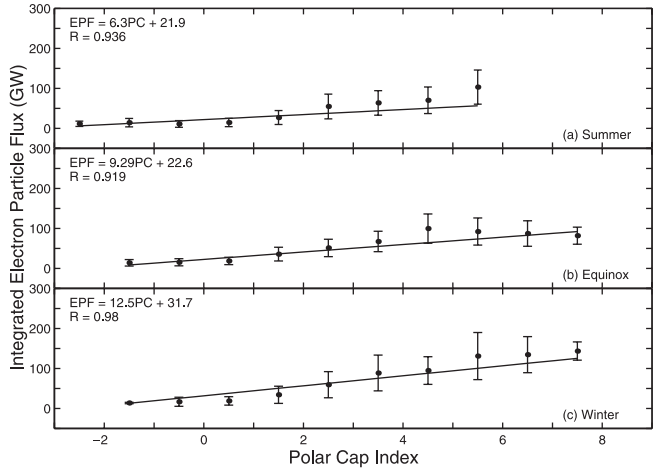

Figure 9. Hemispheric integrated electron particle flux heating for (top) summer, (middle) equinox, and (bottom) winter.

[25] Average polar cap potential is positively correlated when the PC index is positive with correlation coefficients of 0.99 for all three seasons. During summer, when the PC index is negative, the polar cap potential is negatively correlated with a correlation coefficient of −0.879. The slope of the weighted linear fits for all three seasons (17.1, 12.3, and 12.9 for summer, equinox, and winter, respectively) is smaller than that reported by *Troshichev et al.* [1996]. This discrepancy can be accounted for if, for negative PC indices, we convert the polar cap potential into a negative value and include all data into one linear fit (similar to *Troshichev et al.* [1996]). When we do this, we get slopes of 21, 19.1, and 17 for summer, equinox, and winter, respectively, consistent with *Troshichev et al.* [1996]. The fit coefficients for Figure 8 and their corresponding uncertainties are summarized in Table 3.

[26] Finally, we make a comparison of the average Joule heating with the average energy from electron particle flux. We have created average patterns of electron particle flux corresponding to each PC bin in Figures 2, 3, and 4. Three examples of these patterns can be seen in the bottom row of Figure 6, which corresponds to the negative PC bins in summer (top row of Figure 2). Figure 9 is a plot of hemispheric integrated electron particle flux versus PC for summer (top panel), equinox (middle panel), and winter (bottom panel). Corresponding integrated Joule heating rates are plotted in Figure 7 for a comparison. To first order, one can see that Joule heating rates are typically greater than particle flux energy. Electron particle fluxes are linearly correlated with PC with correlation coefficients of 0.94 (summer), 0.92 (equinox), and 0.98 (winter). The weighted linear fit equations are shown in each plot panel and summarized in Table 4. It appears that during quiet periods, with PC close to zero, Joule heating and particle energy are comparable in magnitude. In summer and equinox, as the PC index decreases below zero, Joule heating increases, whereas particle energy appears relatively constant. In winter, however, Joule heating and particle energy appear to match one another, which is perhaps a result that during the winter season, polar cap conductivity, and thus Joule heating, is more dependent on electron particle precipitation during times of negative PC conditions.

[27] Figure 10 is a plot of the ratio of Joule heating to electron particle energy for the three seasons. Summer is indicated by a square, equinox is a triangle, and winter is a circle. From this plot we see that although the spatial distributions of Joule heating and particle energy are very different; they provide, on average, equal contributions to the global energy budget during geomagnetically quiet times (near zero PC). As PC increases in both directions from zero, Joule heating becomes a larger contributor with ratios approaching 4 to 5, consistent with previous studies [*Ahn et al.*, 1983; *Lu et al.*, 1995]. The exception again is negative PCs during winter, where the ratio of Joule heating to particle energy remains close to 1 and is sometimes <1. The heating ratios also exhibit seasonal variations, with the largest ratio occurring in the summer followed by equinox and then winter. In addition, although *Ahn et al.* [1983] and *Vickrey et al.* [1982] showed that the Joule heating to particle energy ratio was independent of the *AL* and *Kp* indices, respectively, it is clear from our data that the ratios are dependent on the PC index.

Table 3. Linear Coefficients and Uncertainties for Polar Cap Potential Versus PC Index ($\Phi_{pc} = a\mathrm{PC} + b$)

	Negative PC		Positive PC	
	a	*b*	*a*	*b*
Summer	−1.14 (±4.7)	39.9 (±2.0)	17.1 (±11.7)	29.5 (±3.1)
Equinox			12.3 (±9.5)	32.7 (±2.2)
Winter			12.9 (±9.5)	29.4 (±2.3)

Table 4. Linear Coefficients and Uncertainties for Electron Particle Flux (EPF) Versus PC Index (EPF = *a*PC + *b*)

	a	*b*
Summer	6.3 (±4.5)	21.9 (±2.3)
Equinox	9.29 (±4.5)	22.6 (±1.9)
Winter	12.5 (±2.9)	31.7 (±1.8)

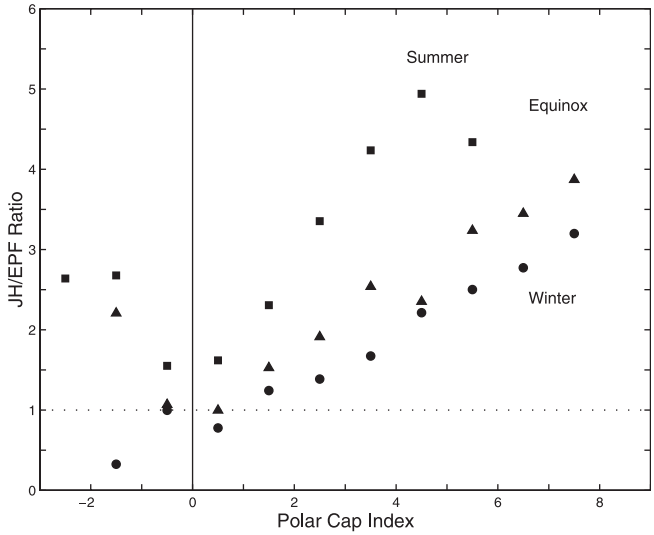

Figure 10. Ratio of Joule heating to electron particle heating as a function of PC. Summer is indicated by a square, equinox by a triangle, and winter by a circle.

4.3. Limitations

[28] We must note some limitations in our data and analysis, in that it is difficult to quantify the effects of neutral winds, electric field variability, and induced currents in the AMIE procedure. Neutral wind effects are known to sometimes enhance the local Joule heating rate upward from 200–400% associated with significant changes in the electric field direction, as well as sometimes reducing the local heating rate by 40% during periods when the electric field is enhanced but in a steady direction [*Thayer*, 1998]. In one study of a Geospace Environment Modeling campaign period, 28–29 March 1992, *Lu et al.* [1995] showed that neutral winds had a 28% reduction on Joule heating. Accurately accounting for neutral winds in our AMIE database would be difficult to accomplish without incorporating AMIE results into a thermosphere-ionosphere general circulation model, similar to the approach taken by *Lu et al.* [1995]. Since AMIE relies heavily on magnetometer data, the AMIE procedure does capture some neutral wind effects since the magnetometers measure magnetic fields from all sources. Separating out the neutral wind effect from other magnetic field sources, however, would be a major undertaking and would be beyond the scope of this paper.

[29] Not accounting for the variability in the electric field can also lead to underestimating Joule heating. Using theoretical arguments, *Codrescu et al.* [1995] showed that by including electric field variability, Joule heating estimates could increase by 33–234% depending on whether the variability was of magnetospheric origin or due to local conductivity changes. Further, *Codrescu et al.* [2000] showed that inclusion of electric field variance (as a Gaussian about a zero mean) into the Millstone Hill electric field model yielded integrated hemispheric Joule heating rates about twice what one would get by just using the average electric field in the Joule heating calculations. Recently, using European Incoherent Scatter radar data, *Rodger et al.* [2001] compared 6-min electric field data to hourly averaged electric field data, and found that the median underestimation of Joule heating by using hourly averaged electric field data was ~20% with an upper extreme of 40%. They also determined that this underestimation was independent of geomagnetic conditions, solar flux, and magnetic local time. Finally, *Crowley and Hackert* [2001] have reported results of temporal variations in AMIE's electric field for a single day. They found that the standard deviation of their patterns was comparable with the mean value of the high-latitude electric field. We have determined (not shown) that the standard deviations in our Joule heating patterns are, at times, on the same order of magnitude as the average Joule heating. However, they are usually lower. Future work will investigate the spatial variability of the electric field in our database.

[30] Another possible limitation of this study could be due to inaccurately accounting for magnetic field contributions from internal sources like induced currents in Earth. A recent study by *Tanskanen et al.* [2001] showed that magnetic contributions from induced currents in Earth can account for up to 40% of the measured magnetic field at a given station during substorm onset. Additionally, during substorm recovery, stations near oceans can receive between 25 and 30% contribution from these internal currents, while inland stations receive between 15 and 20%. Thus AMIE could be overestimating Joule heating.

[31] In summary, we have noted that various uncertainties could perhaps lead to underestimations of AMIE-derived Joule heating (neutral winds and electric field variability) or overestimations (induced currents). Comparisons between AMIE results and runs of the Thermosphere-Ionosphere Electrodynamics General Circulation Model, however, suggest that AMIE generally underestimates upper atmospheric heating by a factor of 2 [*Emery et al.*, 1999].

[32] The AMIE procedure does attempt to account for uncertainty (and possible associated variability) in the data. The procedure accounts for some electric field variability since AMIE uses an inverse covariance matrix of the "errors" to develop weighting factors of its observational data. For instance, AMIE uncertainty in the electric fields ranges from 5 to 25 mV/m that correspond to uncertainties in the Joule heating estimates on the order of a few mW/m^2 [*Richmond and Kamide*, 1988].

[33] In terms of accounting for internal current sources, the AMIE procedure provides a rough estimate of the magnetic field due to induced underground current sources by assuming a perfectly conducting layer at a depth of 250 km below Earth's surface overlain by a perfect insulator. This leads to uncertainties in the magnetic field on the order of 10% [*Richmond and Kamide*, 1988].

[34] Although it would be ideal to account for all of the errors and uncertainties in these 15 AMIE case studies, the data sets and current implementation of the algorithm do not lend themselves to a straightforward means of doing so. Efforts are underway, however, to improve future AMIE analysis by improving and expanding the covariance matrix used in the procedure [*Matsuo et al.*, 2002]. Despite the limitations discussed here we believe the AMIE results, in general, and our results, specifically, are consistent with previous studies that determined average global characteristics of the ionosphere. Further, we anticipate this study

will provide a framework for future comparison of Joule heating derived from more direct measurements obtained from satellites and radars.

5. Conclusions

[35] In this study we have shown averaged estimated patterns of Joule heating from AMIE as a function of the polar cap (PC) index and season. We find that during times of negative PC, reminiscent of a reverse convection situation in the polar cap, Joule heating is confined to a limited region in the dayside high latitude. As geomagnetic activity increases with increasing PC, heating intensifies and expands along the auroral oval with the greatest heating occurring along the dawn and dusk flanks. Moderate to high values of PC are associated with hemispherically integrated Joule heating rates in excess of 450 GW. Joule heating is typically $\sim$4–5 times greater than electron particle heating during geomagnetically active times, but during quiet times the heat inputs are comparable. Seasonal variations are also evident in the ratio of the two heat inputs.

[36] **Acknowledgments.** The PC index was provided by the Danish Meteorological Institute. We thank A. Richmond, O. Troshichev, J. Waterman, and R. Haaland for valuable comments. This research was supported by the Air Force Office of Scientific Research and NSF ATM grant 0077536. Work at HAO/NCAR was partially supported by the NSF Space Weather Program.

[37] Janet G. Luhmann thanks Alan S. Rodger and another referee for their assistance in evaluating this paper.

References

Ahn, B.-H., S.-I. Akasofu, and Y. Kamide, The Joule heat production rate and the particle energy injection rate as a function of the geomagnetic indices *AE* and *AL*, *J. Geophys. Res.*, *88*, 6275–6287, 1983.

Baumjohann, W., and Y. Kamide, Hemispherical Joule heating and the *AE* indices, *J. Geophys. Res.*, *89*, 383–388, 1984.

Chun, F. K., D. J. Knipp, M. G. McHarg, G. Lu, B. A. Emery, S. Vennerstrøm, and O. A. Troshichev, Polar cap index as a proxy for hemispheric Joule heating, *Geophys. Res. Lett.*, *26*, 1101–1104, 1999.

Codrescu, M. V., T. J. Fuller-Rowell, and J. C. Foster, On the importance of *E*-field variability for Joule heating in the high-latitude thermosphere, *Geophys. Res. Lett.*, *22*, 2393–2396, 1995.

Codrescu, M. V., T. J. Fuller-Rowell, J. C. Foster, J. M. Holt, and S. J. Cariglia, Electric field variability associated with the Millstone Hill electric field model, *J. Geophys. Res.*, *105*, 5265–5273, 2000.

Cooper, M. L., C. R. Clauer, B. A. Emery, A. D. Richmond, and J. D. Winningham, A storm time assimilative mapping of ionospheric electrodynamics analysis for the severe geomagnetic storm of November 8–9, 1991, *J. Geophys. Res.*, *100*, 19,329–19,342, 1995.

Crowley, G., and C. L. Hackert, Quantification of high latitude electric field variability, *Geophys. Res. Lett.*, *28*, 2783–2786, 2001.

Crowley, G., A. J. Ridley, D. Deist, S. Wing, D. J. Knipp, B. A. Emery, J. Foster, R. Heelis, M. Hairston, and B. W. Reinisch, Transformation of high-latitude ionospheric F-region patches into blobs during the March 21, 1990 storm, *J. Geophys. Res.*, *105*, 5215–5230, 2000.

Emery, B. A., C. Lathuillere, P. G. Richards, R. G. Roble, M. J. Buonsanto, D. J. Knipp, P. Wilkinson, D. P. Sipler, and R. Niciejewski, Time dependent thermospheric neutral response to the 2–11 November 1993 storm period, *J. Atmos. Sol. Terr. Phys.*, *61*, 329–350, 1999.

Farrugia, C. J., et al., Geoeffectiveness of three WIND magnetic clouds: A comparative study, *J. Geophys. Res.*, *103*, 17,261–17,278, 1998.

Foster, J. C., J.-P. St.-Maurice, and V. J. Abreu, Joule heating at high latitudes, *J. Geophys. Res.*, *88*, 4885–4896, 1983.

Knipp, D. J., et al., Ionospheric convection response to slow, strong variations in a northward interplanetary magnetic field: A case study for January 14, 1988, *J. Geophys. Res.*, *98*, 19,273–19,292, 1993.

Knipp, D. J., et al., An overview of the early November 1993 geomagnetic storm, *J. Geophys. Res.*, *103*, 26,197–26,220, 1998.

Kobea, A. T., A. D. Richmond, B. A. Emery, C. Peymirat, H. Lühr, T. Moretto, M. Hairston, and C. Amory-Mazaudier, Electrodynamic coupling of high and low latitudes: Observations on May 27, 1993, *J. Geophys. Res.*, *105*, 22,979–22,989, 2000.

Lu, G., et al., Interhemispheric asymmetry of the high-latitude ionospheric convection pattern, *J. Geophys. Res.*, *99*, 6491–6510, 1994.

Lu, G., A. D. Richmond, B. A. Emery, and R. G. Roble, Magnetosphere-ionosphere-thermosphere coupling: Effect of neutral winds on energy transfer and field-aligned current, *J. Geophys. Res.*, *100*, 19,643–19,659, 1995.

Lu, G., et al., High-latitude ionospheric electrodynamics as determined by the assimilative mapping of ionospheric electrodynamics procedure for the conjunctive SUNDIAL/ATLAS 1/GEM period of March 28–29, 1992, *J. Geophys. Res.*, *101*, 26,697–26,718, 1996.

Lu, G., et al., Global Energy deposition during the January 1997 magnetic cloud event, *J. Geophys. Res.*, *103*, 11,685–11,694, 1998.

Matsuo, T., A. D. Rickmond, and D. W. Nychka, Modes on high-latitude electric field variability derived from DE-2 measurements: Empirical orthogonal function (EOF) analysis, *Geophys. Res. Lett.*, *29*, 10.1029/2001GL014077, 2002.

Pinnock, M., A. S. Rodger, K. B. Baker, G. Lu, and M. Hairston, Conjugate observations of the day side reconnection electric field: A GEM boundary layer campaign, *Ann. Geophys.*, *17*, 443–454, 1999.

Richardson, I. G., E. W. Cliver, and H. V. Cane, Sources of geomagnetic activity over the solar cycle: Relative importance of coronal mass ejections, high-speed streams, and slow solar wind, *J. Geophys. Res.*, *105*, 18,203–18,213, 2000.

Richmond, A. D., and Y. Kamide, Mapping electrodynamic features of the high-latitude ionosphere from localized observations: Technique, *J. Geophys. Res.*, *93*, 5741–5759, 1988.

Rodger, A. S., G. D. Wells, R. J. Moffett, and G. J. Bailey, The variability of Joule heating, and its effects on the ionosphere and thermosphere, *Ann. Geophys.*, *19*, 773–781, 2001.

Tanskanen, E. I., A. Viljanen, T. I. Pulkkinen, R. Pirjola, L. Häkkinen, A. Pulkkinen, and O. Amm, At substorm onset, 40% of *AL* comes from underground, *J. Geophys. Res.*, *106*, 13,119–13,134, 2001.

Taylor, J. R., T. K. Yeoman, M. Lester, B. A. Emery, and D. J. Knipp, Variations in the polar cap area during intervals of substorm activity on 20–21 March 1990 deduced from AMIE convection patterns, *Ann. Geophys.*, *14*, 879–887, 1996.

Taylor, J. R., M. Lester, T. K. Yeoman, B. A. Emery, D. J. Knipp, D. Orr, S. I. Solovyev, T. J. Hughes, and H. Luhr, The response of the magnetosphere to the passage of a coronal mass ejection on March 20–21, 1990, *Ann. Geophys.*, *15*, 671–684, 1997.

Thayer, J. P., Height-resolved Joule heating rates in the high-laitude *E* region and the influence of neutral winds, *J. Geophys. Res.*, *103*, 471–487, 1998.

Troshichev, O. A., V. G. Andresen, S. Vennerstrøm, and E. Friis-Christensen, Magnetic activity in the polar cap: A new index, *Planet. Space Sci.*, *36*, 1095–1102, 1988.

Troshichev, O. A., H. Hayakawa, A. Matsuoka, T. Mukai, and K. Tsuruda, Cross polar cap diameter and voltage as a function of PC index and interplanetary quantities, *J. Geophys. Res.*, *101*, 13,429–13,435, 1996.

Vennerstrøm, S., E. Friis-Christensen, O. A. Troshichev, and V. G. Andresen, Comparison between the polar cap index, PC, and the auroral electrojet indices *AE*, *AL*, and *AU*, *J. Geophys. Res.*, *96*, 101–113, 1991.

Vickrey, J. F, R. R. Vondrak, and S. J. Matthews, Energy deposition by precipitating particles and Joule dissipation in the auroral ionosphere, *J. Geophys. Res.*, *87*, 5184–5196, 1982.

F. K. Chun, D. J. Knipp, J. R. Lacey, and M. G. McHarg, Department of Physics, U.S. Air Force Academy, 2354 Fairchild Drive, Suite 2A31, CO 80840, USA. (Francis.Chun@usafa.af.mil; Delores.Knipp@usafa.af.mil; Matthew.Mcharg@usafa.af.mil)

G. Lu and B. A. Emery, High Altitude Observatory, National Center for Atmospheric Research, P.O. Box 3000, Boulder, CO 80307, USA. (ganglu@ncar.ucar.edu; emery@ncar.ucar.edu)

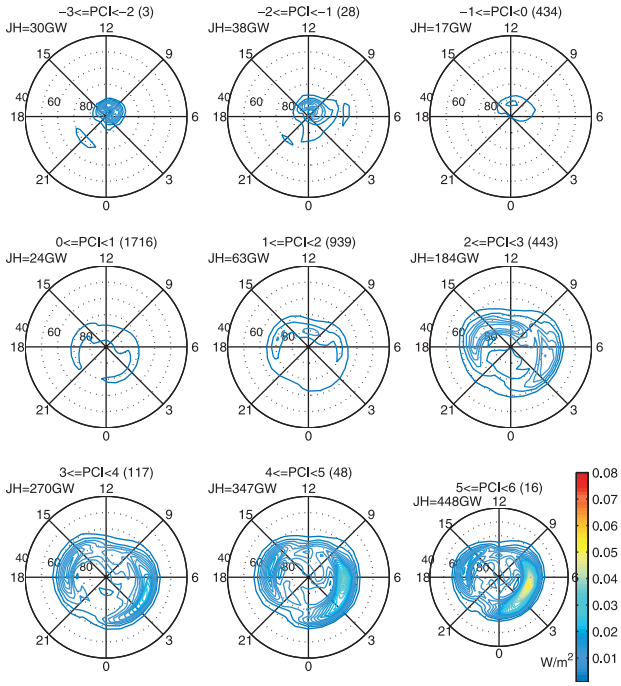

Figure 2. Average Joule heating patterns as a function of polar cap index (summer).

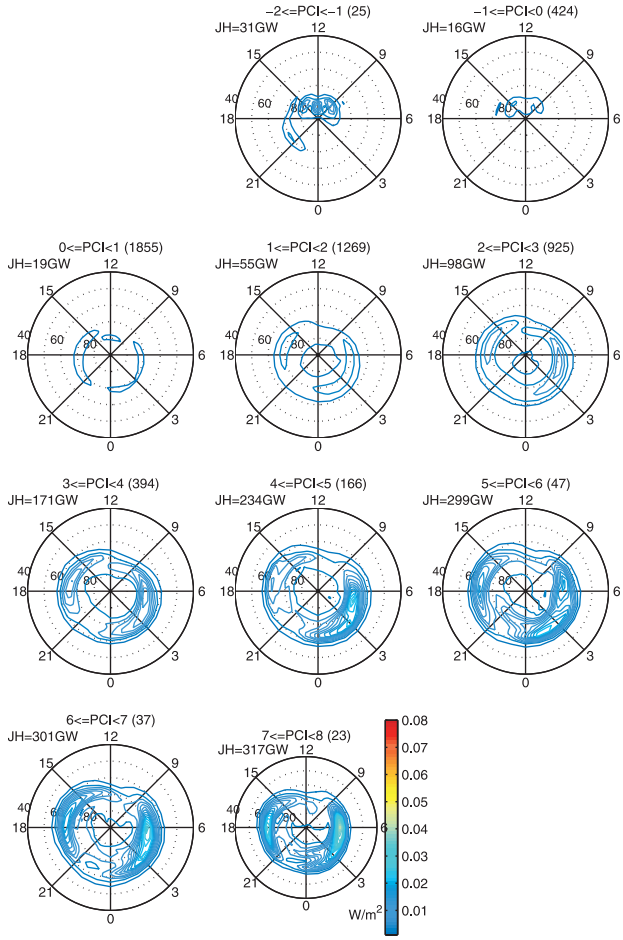

Figure 3. Average Joule heating patterns as a function of PC index (equinox).

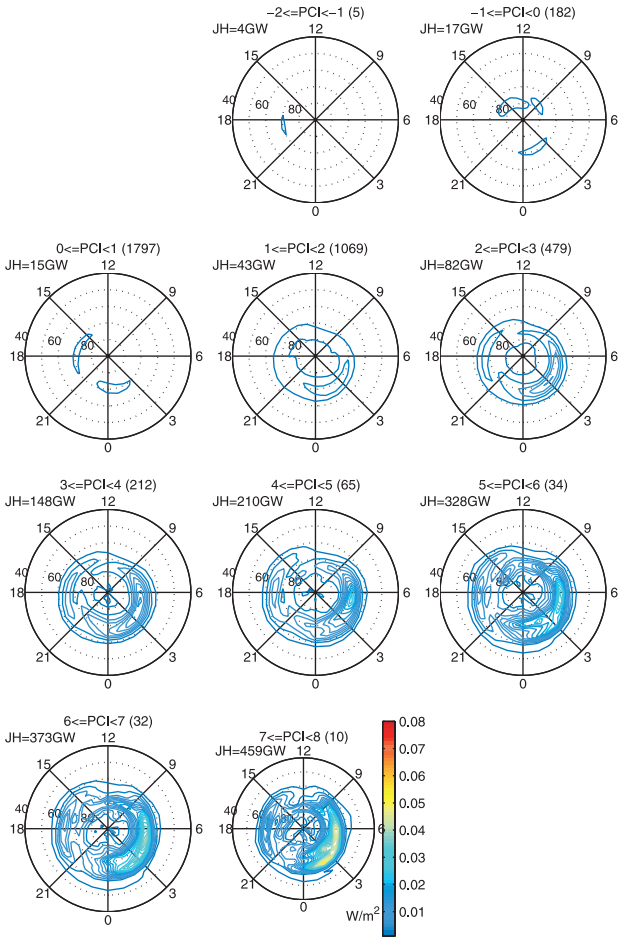

Figure 4. Average Joule heating patterns as a function of PC index (winter).

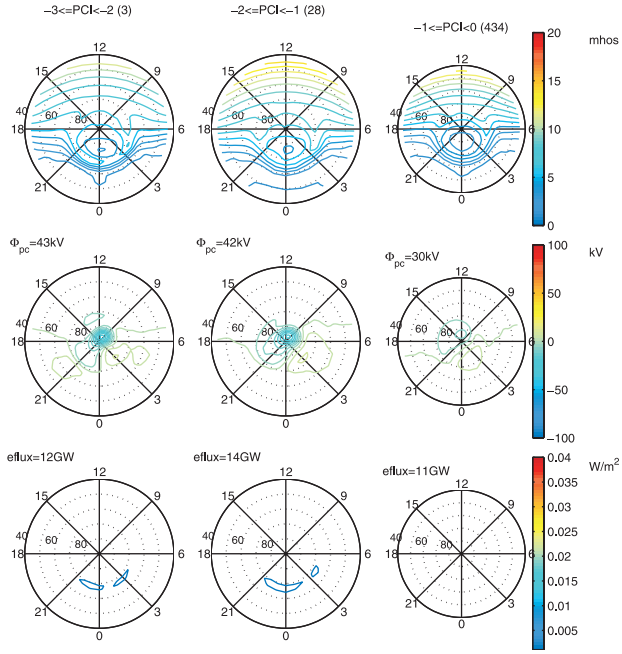

Figure 6. Average Pedersen conductance and electric potential patterns associated with the averaged Joule heating summer patterns (top row of plots in Figure 2) for negative PC ($-2.5 \leq \mathrm{PC} < -0.5$). The average electron particle flux patterns corresponding to the same PC bins are plotted in the bottom row.